Petroleum Science 19 (2022) 1390–1400

Contents lists available at ScienceDirect

Petroleum Science

journal homepage: www.keaipublishing.com/en/journals/petroleum-science

Original Paper

Study on the mechanism of hydrodesulfurization of tetrahydrothiophene catalyzed by nickel phosphide

Chuan-Tao Zhu, Li-Qiang Zhang, Mei-Ling Zhou, Xin-Wei Wang, Zheng-Da Yang, Ri-Yi Lin*, De-Wei Yang

College of New Energy, China University of Petroleum, Qingdao, 266580, China

ARTICLE INFO

Article history:
Received 24 February 2021
Accepted 13 August 2021
Available online 30 October 2021

Edited by Xiu-Qiu Peng

Keywords:
Tetrahydrothiophene
Nickel phosphide
Hydrodesulfurization
Hydrogen sulfide
DFT

ABSTRACT

Hydrodesulfurization (HDS) reaction can significantly reduce the viscosity and sulfur content of heavy oil, while the HDS reaction mechanism of tetrahydrothiophene as the main sulfide in heavy oil is still unclear. The HDS experiment of tetrahydrothiophene catalyzed by nickel phosphide (Ni_2P) is carried out at 200–300 °C. The results indicate that the H_2S production under the catalysis of Ni_2P increases obviously within 200–250 °C. The main gas products of HDS reaction are butane, butene and H_2S. Meanwhile, the mechanism of tetrahydrothiophene catalyzed by Ni_2P is analyzed based on Density Functional Theory (DFT). It is revealed that the adsorption model is most stable when tetrahydrothiophene is vertically adsorbed on the V–Ni-Hcp1 site of Ni_2P (001). The C–S bond is elongated and the C–C bond is shortened after adsorption. Hydrogenation (HYD) is the most possible reaction route of tetrahydrothiophene on Ni_2P (001) surface. There are two routes with the lowest activation energy, which are $C_4H_8S \rightarrow C_4H_8SH^* \rightarrow C_4H_9SH^* \rightarrow C_4H_{10}+H_2S$ and $C_4H_8S \rightarrow C_4H_9S^* \rightarrow C_4H_9^*+SH^* \rightarrow C_4H_{10}+H_2S$. Butane and H_2S are produced in the reaction, corresponding to the experimental results. This study provides a basis for understanding of the HDS mechanism of tetrahydrothiophene catalyzed by Ni_2P.

© 2021 The Authors. Publishing services by Elsevier B.V. on behalf of KeAi Communications Co. Ltd. This is an open access article under the CC BY-NC-ND license (http://creativecommons.org/licenses/by-nc-nd/4.0/).

1. Introduction

Heavy oil is one of main energy source that countries have high hope for in the 21st century. However, the extremely high viscosity of heavy oil and the presence of sulfur have brought serious challenges to its exploitation. It is necessary and urgent to reduce the viscosity and sulfur content of heavy oil due to the environmental pressure, stricter international environmental regulations (Zuriaga-Monroy et al., 2009). Thermal recovery is the main method of heavy oil recovery (Mokheimer et al., 2019). The injected high temperature fluid increased the reservoir temperature and reduced the viscosity of heavy oil. Meanwhile, aquathermolysis reaction occurred between water and heavy oil (Clark and Hyne, 1990). Hyne (1986) proposed that hydrodesulfurization (HDS) was the last step of the aquathermolysis reaction, in which the C–S bond broke and formed hydrogen sulfide with hydrogen in the system, and reduced the sulfur content in heavy oil. Although the viscosity and sulfur content of heavy oil are reduced under the action of hydrothermal treatment, it still cannot meet the actual demand, and other measures need to be further taken.

According to the current research, adding catalyst is one of the effective means to promote HDS reaction, and the mechanism of its reaction was studied (Oyama, 2003; Oyama et al., 2009). Since it is difficult to theoretically analyze the HDS reaction process due to the complex composition of heavy oil, thiophene sulfides are the main sulfides in heavy oil and commonly used to replace heavy oil (Jin et al., 2018; Liu et al., 2015). Generally, transition metals are currently used as cocatalysts, and the CoMo or NiMo bimetallic catalyst systems supported by Al_2O_3 or SiO_2 have been used in industry (Ahmed et al., 2011; Da Silva Neto et al., 2016; Wang et al., 2017). However, Boukoberine et al. (Boukoberine and Hamada, 2016) found that the CoMo/c-Al_2O_3–CuY catalyst reduced the HDS activity of thiophene by increasing the loading of CuY zeolite. Phosphide catalyst, which has not been widely used, has high activity in hydrodesulfurization (Oyama et al., 2009). Oyama (2003) proposed that the desulfurization activity of different phosphors in DBT was Fe_2P < CoP < MoP < WP < Ni_2P, and Ni_2P has higher activity in HDS and HDN reaction. Sawhill et al. (Sawhill, 2003)

* Corresponding author.
E-mail address: linry@upc.edu.cn (R.-Y. Lin).

https://doi.org/10.1016/j.petsci.2021.10.023
1995-8226/© 2021 The Authors. Publishing services by Elsevier B.V. on behalf of KeAi Communications Co. Ltd. This is an open access article under the CC BY-NC-ND license (http://creativecommons.org/licenses/by-nc-nd/4.0/).

found that the HDS activity of Ni_2P/SiO_2 catalysts by pretreatment with He was 15 and 3.5 times higher than that of Mo/SiO_2 and $NiMo/SiO_2$ catalysts, respectively. It has been demonstrated that Ni_2P, as HDS catalyst with high activity, has great hydrogenation selectivity (Song et al. 2013, 2019; Lan et al., 2016).

Oyama et al. (Oyama and Lee, 2008) considered that the direct desulfurization (DDS) mainly occurred at Ni (1) site and hydrogenation (HYD) of thiophene mainly occurred at Ni (2) site in HDS reaction catalyzed by Ni_2P. Li et al., (2017) calculated that DDS is a possible HDS reaction route of thiophene on MoP (001) surface doped with S atom. Wang et al., (2017) prepared $NiAl/\gamma\text{-}Al_2O_3$ catalyst and showed that HYD was the main reaction route in the HDS reaction network of 4,6-DMDBT. Bando et al., (2012) revealed that tetrahydrothiophene (THT) was detected as a reaction intermediate and NiPS was the actual reactive phase in the Ni_2P/McM-41 catalytic thiophene HDS reaction.

The mechanism of hydrodesulfurization catalyzed by Ni_2P is mainly studied by thiophene. While tetrahydrothiophene occupies a certain proportion in thiophene sulfides, which is different from the molecular structure of thiophene and does not have C—C double bond. In order to comprehensively reveal the HDS mechanism of heavy oil catalyzed by Ni_2P, it is necessary to further study the HDS mechanism of tetrahydrothiophene catalyted by Ni_2P.

Therefore, tetrahydrothiophene was used as the model compound and Ni_2P was used as the catalyst to carry out the HDS experiment at different time and temperature in this study. The HDS process of THT on the surface of Ni_2P was simulated and the mechanism of HDS catalyzed by Ni_2P was explored based on Density Functional Theory (DFT). By combining the experimental results with the theoretical calculations, this research was expected to improve the understanding of HDS reaction mechanism network of heavy oil, and provided theoretical basis for the desulfurization and viscosity reduction technology of heavy oil.

2. Experiment and simulation

2.1. Catalysts characterization

Preparation method of Ni_2P catalyst. 2.376 g $NiCl_2{\cdot}6H_2O$ and 0.760 g NaH_2PO_2 were dissolved in 25 mL deionized water. The mixture was stirred for 4 h and dried at 90 °C for 12 h. Then calcined at 300 °C for 30 min at 5 °C/min in Ar atmosphere. Finally, the powder was repeatedly washed with deionized water and anhydrous ethanol, and dried at 120 °C for 3 h.

The Ni_2P catalyst samples were characterized by X-ray diffraction (XRD) and X-ray photoelectron spectroscopy (XPS). The XPS and XRD test results of Ni_2P are shown in Fig. 1. As shown in Fig. 1a, the diffraction peaks were wide, which proved that the prepared Ni_2P was a crystal structure with small grains, and there were several obvious diffraction peaks at $2\theta = 40.7°$, 44.6°, 47.3°, 54.2°, 54.9°, which was the same as the standard spectrum of Ni_2P, indicating the active phase is mainly Ni_2P.

As shown in Fig. 1b, the core spectrum of Ni 2p consists of three components. The first of which centered at 853.2 eV can be considered to $Ni^{\delta+}$ species in the Ni_2P phase. The second at 856.7 eV corresponded to the possible interaction between Ni^{2+} species and phosphate species, which was the result of surface passivation, and the 862.5 eV was the satellite peak of Ni $2p_{2/3}$ (Kuhn et al., 2008). The third at 875.2 eV corresponded to Ni $2p_{1/2}$ and its satellite peak at 881.3 eV (Song et al., 2011). As shown in Fig. 1c, the peak at 129.8 eV could be attributed to the $P^{\delta-}$ species in the Ni_2P phase (Zhang et al., 2016), and the peak at 133.6 eV could be attributed to phosphate (P^{5+}), because the surface oxidation of Ni_2P particles occurs (Kanama, 2001).

2.2. Ni_2P catalyzed tetrahydrothiophene experiment

Aquathermolysis is the main reaction type of H_2S generation at 200–300 °C and thermal cracking is dominant above 300 °C (Zhang et al., 2020). Therefore, the tetrahydrothiophene hydrodesulfurization experiment was conducted at 200–300 °C. Thermal cracking reaction of tetrahydrothiophene was used as contrasts due to a certain degree of tetrahydrothiophene thermal cracking reaction is inevitable.

The thermal cracking and HDS reaction of tetrahydrothiophene with different conditions (Time = 6, 12, 24, 48, 72 h and Temperature = 200, 225, 250, 275, 300 °C) were studied. Schematic of the experimental setup (Ma et al., 2019) is shown in Fig. 2. The weighed amount of tetrahydrothiophene (2 g) and Ni_2P (0.2 g) were added to the reaction still, and filled with 1 MPa hydrogen. The H_2S production was measured by an on-line H_2S detector and the other gas collected by the gas bag was detected by FID/TCD gas chromatography analyzer. The samples after reaction were subjected to solid-liquid separation, and the compositions and contents of the collected liquid phase were detected by Gas Chromatography-Mass Spectrometer (GC-MS).

2.3. Computational details

2.3.1. DFT calculation

The calculations were performed by using $Dmol^3$ module in Material Studio software. The electron exchange correlation potential was calculated by the generalized-gradient approximation (GGA)-PW91 (Perdew and Yue, 1986). Core Treatment was selected all the electrons in the All Electron Relativistic treatment system. The valence electron wave function was expanded by the double numerical basis sets plus polarization function (DNP). The Monkhorst-Pack grid parameter of the Brillouin zone integration was set to Fine. The Methfessel-Paxton smearing value was 0.005 Ha. The convergence precision was set as energy change less than 1×10^{-5} Ha, atomic displacement was less than 2×10^{-3} Å, and atomic force was less than 5×10^{-3} Ha/Å. The effect of spin polarization on adsorption configuration was negligible (Ge et al., 2000).

2.3.2. Construction and optimization of tetrahydrothiophene molecule and Ni_2P cell

The configurations of tetrahydrothiophene molecule and Ni_2P cell are shown in Fig. 3. Ni_2P is a hexagonal crystal structure and the lattice parameters of Ni_2P are a = b = 5.859 Å, c = 3.382 Å. After the initial model is built, the structure of tetrahydrothiophene molecule and Ni_2P cell is optimized. The lattice parameters of Ni_2P after optimization are a = b = 5.891 Å, c = 3.297 Å, which are consistent with the experimental values (Ge et al., 2000; Rundqvist et al., 1962). The maximum relative error is less than 2%, and the bond length is summarized as shown in Fig. 4. The energy of a tetrahydrothiophene molecule is $E_{THT} = -556.540$ Ha and a Ni_2P cell (6 Ni atoms and 3 P atoms) is $E_{bulk} = -10122.687$ Ha after optimization.

2.3.3. Ni_2P slab model calculation and selection

The surface density of Ni_2P (001) surface was the largest, and the corresponding surface spacing was also the largest. Therefore, the Ni_2P (001) surface was more likely to break and exposed to the catalyst surface. The Ni_2P (001) surface belonged to a low exponent crystal surface, and its surface formation energy was smaller (Liu and Rodriguez, 2005; Wei et al., 2019). The Ni_2P (001) surface was a cycle of two layers of atoms, and each atom layer could be used as a terminal atom layer in a cycle, so there were two different terminal surfaces of Ni_2P (001) surface, namely Ni_3P_2 and Ni_3P (Lin et al., 2020).

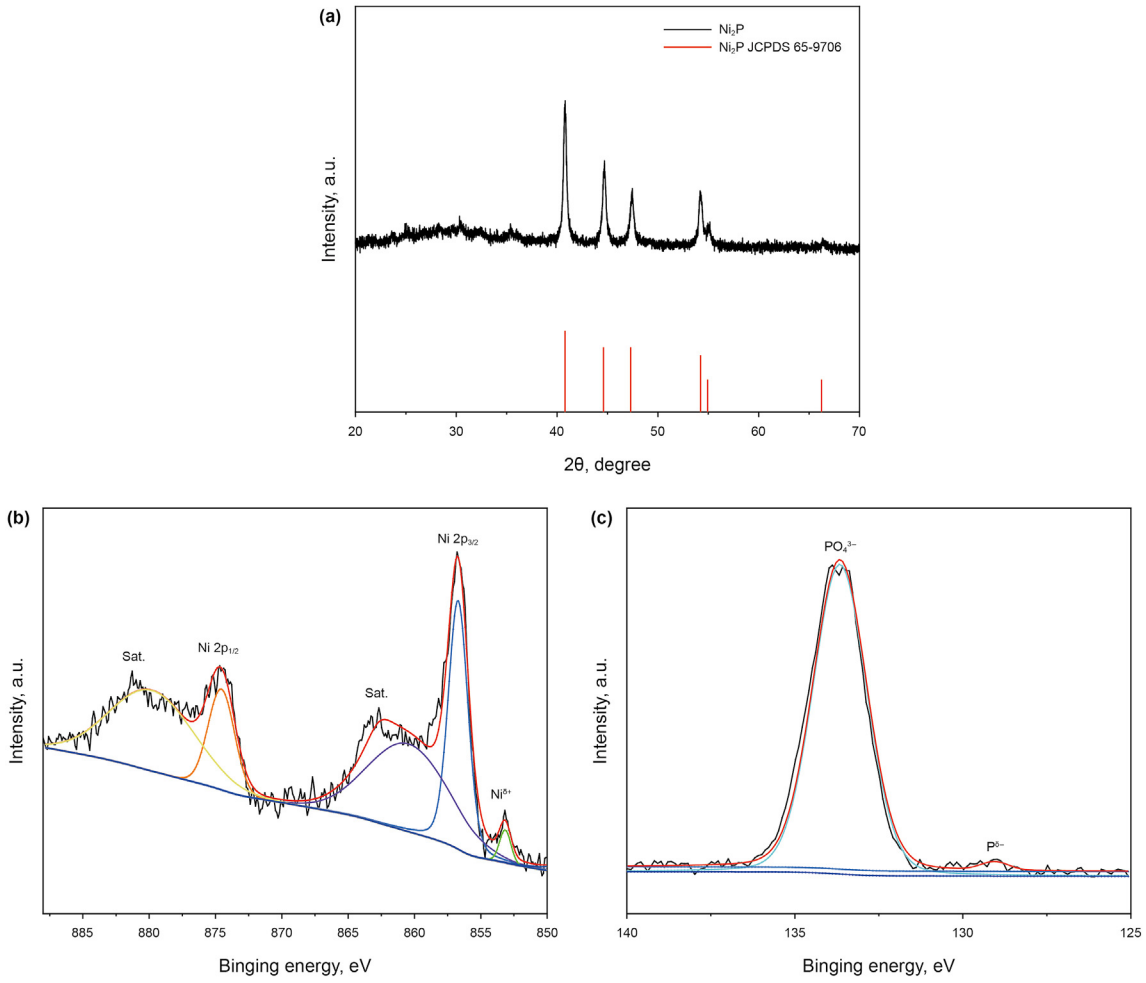

Fig.1. a. XRD patterns of Ni_2P b. XPS spectra of Ni 2p region c. XPS spectra of P 2p region.

The slab model needed to have enough atomic layers to indicate the properties of the bulk phase material, and the number of atomic layers was calculated as 2, 4 and 6 layers. The z-direction vacuum layer thickness was set to be 12 Å, 15 Å, 18 Å and 20 Å to avoid the inter-layer interaction. 1 layer or 2 layers bottom atoms were fixed, and the other atomic layers could be to relax. The convergence test and calculation of the slab model were all low coverage 2 × 2 periodic slab models. Therefore, a total of 48 slab models were constructed. The surface energy was calculated using the following equation:

$$E_{surf} = (E_{slab} - nE_{bulk}) / 2S \quad (1)$$

where E_{slab} is the energy of the surface model; E_{bulk} is the energy of a cell in a body phase; S is the surface area of the slab model; n is the number of cells corresponding to the slab model; E_{surf} is the surface energy. The surface energy data of all slab models are shown in Appendix Table s1.

The surface energy of the slab model with Ni_3P_2 section as the terminal surface was basically smaller than that of Ni_3P under the same conditions. The surface energy of the Ni_3P_2 section was more stable than that of Ni_3P (Liu et al., 2017). The surface energy of the slab model changed little with the change of the vacuum layer thickness, indicating that these changes in the vacuum layer thickness had little influence on the surface energy. The maximum surface energy variation of the slab model was less than 1.6 eV/nm^2 when the number of atomic layers goes from 2 to 6. In addition, the difference of atomic surface energy of 4 or 6 layers was less than 0.04 eV/nm^2 when Ni_3P_2 section was used as the terminal surface.

Therefore, the terminal surface of the slab model in the direction of Ni_2P (001) was represented by Ni_3P_2. The model had 4 layers atoms, 2 layers bottom atoms were fixed, and the vacuum layer

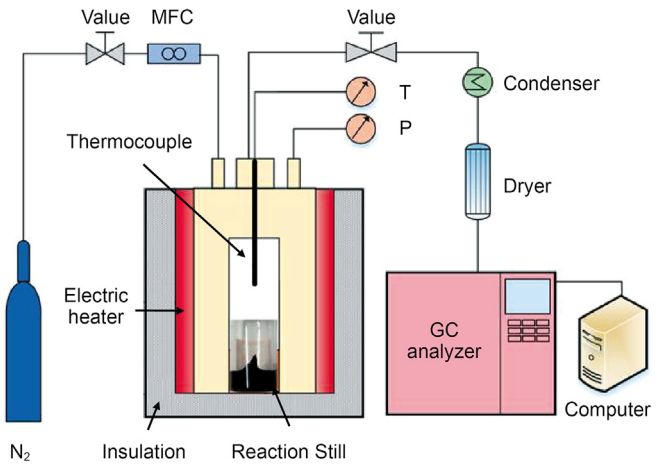

Fig.2. Schematic of the experimental setup.

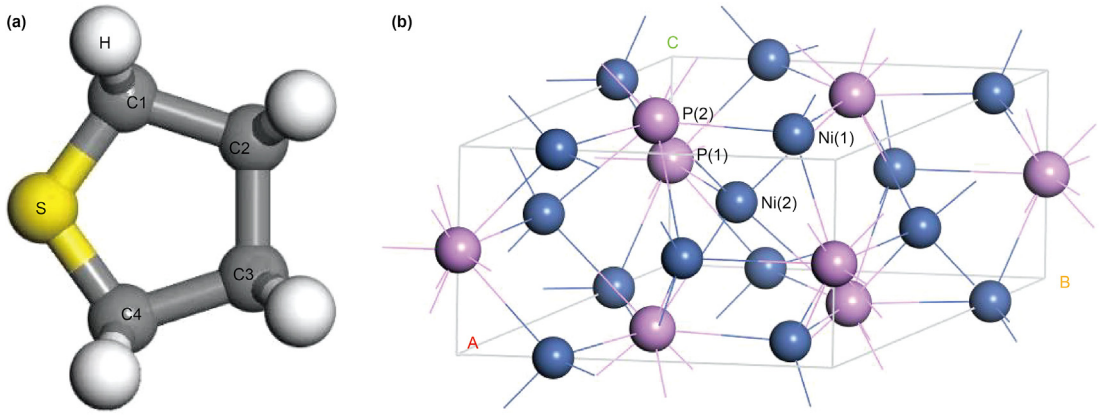

Fig.3. Illustrations of THT molecule (a) and Ni_2P cell (b).

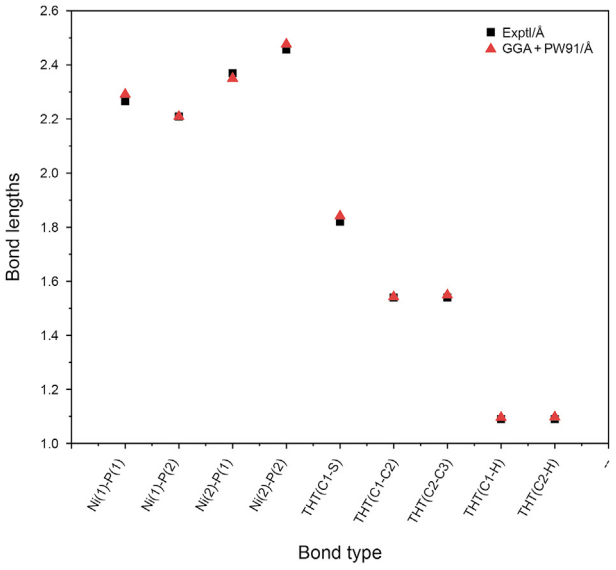

Fig.4. Comparison of experimental and optimized values of bond lengths of THT and Ni_2P.

thickness was 12 Å.

2.3.4. Adsorption energy of reactant on Ni_2P (001) surface

The adsorption configuration was constructed on the 4 layers surface model of Ni_3P_2. Adsorption position of tetrahydrothiophene on Ni_2P (001) surface is shown in Fig. 5. There are two Top positions, two Hcp positions and one Bridge position. Sixteen adsorption configurations were calculated when tetrahydrothiophene was parallelly adsorbed on Ni_2P (001) surface, and eleven adsorption configurations were calculated when tetrahydrothiophene was vertically adsorbed on Ni_2P (001) surface at S-terminal.

The adsorption configurations of the Ni-Hcp1 position under parallel adsorption is shown in Fig. 6, and the other adsorption configurations are shown in Appendix Fig. s1. The adsorption energy was calculated using the following equation:

$$E_{ads} = E_{adsorbate/slab} - (E_{absrobate} + E_{slab}) \quad (2)$$

where $E_{absrobate}$ is the energy of the adsorbed unit, Ha; E_{slab} is the base energy, Ha; $E_{adsorbate/slab}$ is the total energy of the surface adsorption system, Ha.

3. Results and discussion

3.1. HDS experiment of THT catalyzed by Ni_2P

3.1.1. Reaction rate of HDS and thermal cracking

H_2S concentration detected after HDS experiment was 9587 mL/m^3 (t = 6 h and T = 200 °C). Moreover, H_2S concentrations in other reaction conditions of HDS experiment were exceeded 10000 mL/m^3 (beyond the range of the instrument). The reaction time was changed to 1h, and H_2S concentration was still close to 10000 mL/m^3 in order to determine the specific concentration of H_2S. Therefore, the reaction time was reduced to 0.75 h and amounts of tetrahydrothiophene and Ni_2P were reduced to 0.5 g and 0.05 g, respectively. The H_2S concentration of tetrahydrothiophene thermal cracking and HDS experiment are shown in Fig. 7. Ni_2P has a

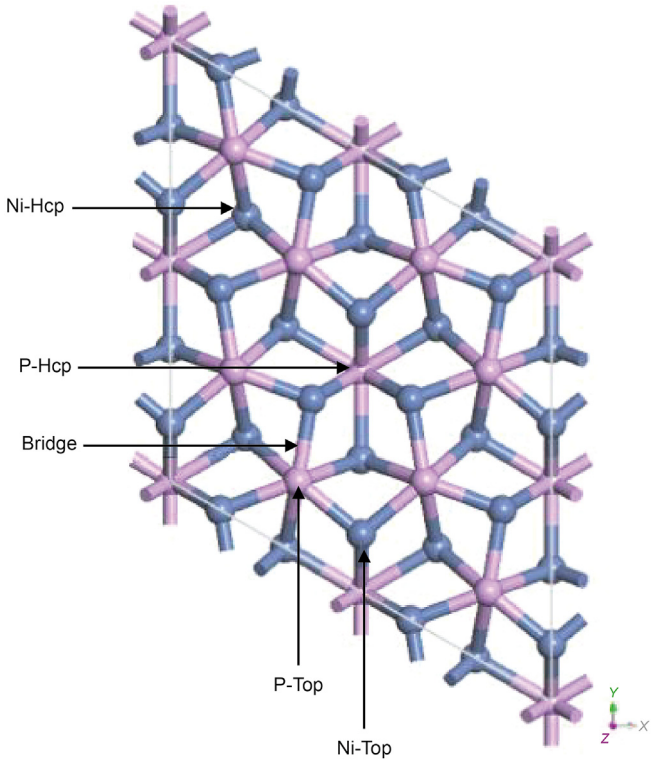

Fig.5. Adsorption position of tetrahydrothiophene on Ni_2P (001) surface.

certain catalytic effect on thermal cracking according to H_2S production by thermal cracking experiments at 250 °C and 300 °C. However, the thermal cracking reaction rate is far lower than HDS reaction, even when the reaction time and tetrahydrothiophene content are reduced. Therefore, the HDS experiment is the major reaction of the H_2S production (Zhao et al., 2016), and its experimental results are mainly analyzed.

3.1.2. Analysis of gas phase products in HDS

The gas phase products of hydrodesulfurization reaction are shown in Fig. 8. Fig. 8a–c are the changes of gas content after reaction for 0.75 h (No Ni_2P), 0.75 h (Add Ni_2P) and 1 h (Add Ni_2P) at 200–300 °C, and Fig. 8d is the change of H_2S concentration. When the reaction time is 1 h, the degree of HDS deepens with the increase of temperature, and H_2 is consumed to generate H_2S and C4 hydrocarbon. However, the detailed concentration of H_2S is not obtained after 250 °C. According to the change of H_2 and C4 hydrocarbon contents in Fig. 8c, the H_2S concentration continues to increase at 275–300 °C.

As shown in Fig. 8a–d, the change of H_2S concentration, H_2 and C4 hydrocarbon contents are not obvious with the increase of temperature when Ni_2P is added at 0.75 h, whereas the H_2S concentration increases gradually when Ni_2P is not added at 0.75 h. Whether or not Ni_2P is added, the H_2S concentration is close at 250–300 °C. It could be inferred that the HDS reaction reaches the maximum degree when Ni_2P is added in the reaction time of 0.75 h, while the HDS reaction reaches the same state with the increase of temperature when the catalyst is not added.

The butane content increases with the increase of temperature. However, the butene content increases at 200–225 °C and decreases at 225–300 °C when the reaction time is 0.75 h. Because of the surplus hydrogen, it is speculated that the decrease of butene content is due to the hydrogenation saturation reaction. When the reaction time is 1 h, the content of butane and butene keeps rising simultaneously due to less amount of hydrogen without hydrogenation saturation reaction.

Therefore, the HDS reaction of tetrahydrothiophene mainly produces H_2S, butene and n-isobutane. The C1–C3 gas content is extremely small. It is speculated that the thermal cracking of trace tetrahydrothiophene occurs during the reaction. C5 and C6+ are detected, shows that there is a certain degree of polymerization reaction (Yi et al., 2009).

3.1.3. Liquid phase product analysis

The liquid phase product of thermal cracking and HDS reaction are shown in Fig. 9. Tetrahydrothiophene (C_4H_8S), Thiophene (C_4H_4S), 2,5-dihydrothiophene (C_4H_6S) and 2-methyltetrahydrothiophene ($C_5H_{10}S$), C_8S sulfur compounds ($C_8H_{12}S_2$: 2,5-methyl-2H-thieno (3,2-b) thian and $C_8H_{14}S_2$: 1,4-bis (ethylthio) butyl-2-yne) are detected.

The mass fraction of tetrahydrothiophene reaches 98% at 1h because of the imminent depletion of H_2. The reaction degree of tetrahydrothiophene reaches the maximum with the increase of temperature at 0.75 h. It is speculated that there is a small amount of surplus or depleted of tetrahydrothiophene. However, the content of tetrahydrothiophene is very high. The liquid phase of thermal cracking is detected in order to determine the reason. The content of tetrahydrothiophene is also reached 98%.

The thiophene C_4H_4S and 2,3-dihydrothiophene C_4H_6S are detected in HDS reaction come from thermal cracking. The other liquid phases are consistent except 1,6-heptadyne (C_7H_8) and p-xylene (C_8H_{10}) detected by thermal cracking. C8 sulfides are produced by polymerization reaction during HDS and thermal cracking, and the content of C8 sulfide increases with the increase of reaction time. Dehydrogenation reaction is occurred in tetrahydrothiophene thermal cracking, and thiophene C_4H_4S and 2,3-dihydrothiophene C_4H_6S are generated in the process of generating H_2S, corresponding to the gas phase detection results (Gould, 1983).

We speculate that the liquid product in HDS reaction comes from thermal cracking and HDS reaction does not produce liquid products. The proportion of generated liquid phases are small due to the small degree of thermal cracking. Therefore, the content of tetrahydrothiophene is reached 98% after reaction.

3.2. HDS simulation of THT catalyzed by Ni_2P

3.2.1. Reactants adsorbed on Ni_2P (001)

(1) Adsorption energy and geometry

Adsorption energy obtained by optimization of the adsorption system is shown in Fig. 10. The adsorption energy of v-Ni-Hcp1 adsorption site in vertical adsorption mode is the largest and more stable. The length of C1–S and C4–S bonds increases from 1.841 Å before adsorption to 1.872 Å and 1.866 Å under the optimal

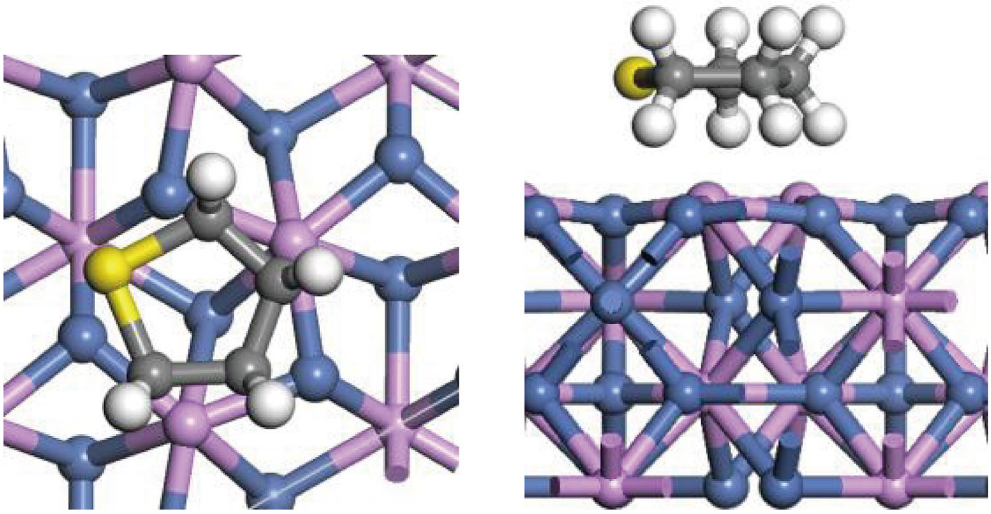

Fig.6. Illustrations of adsorption sites of THT absorbed on Ni_2P (001) surface.

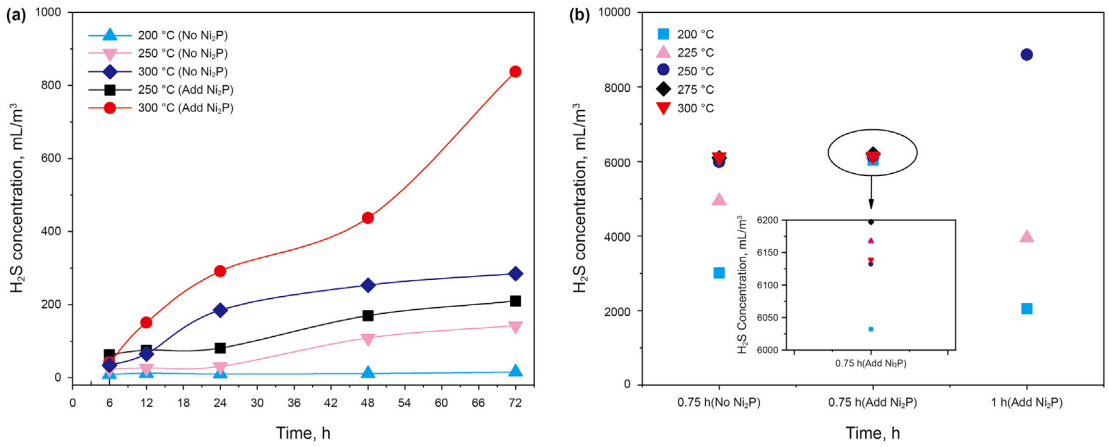

Fig.7. H_2S concentration (a. Thermal cracking, b. HDS of THT).

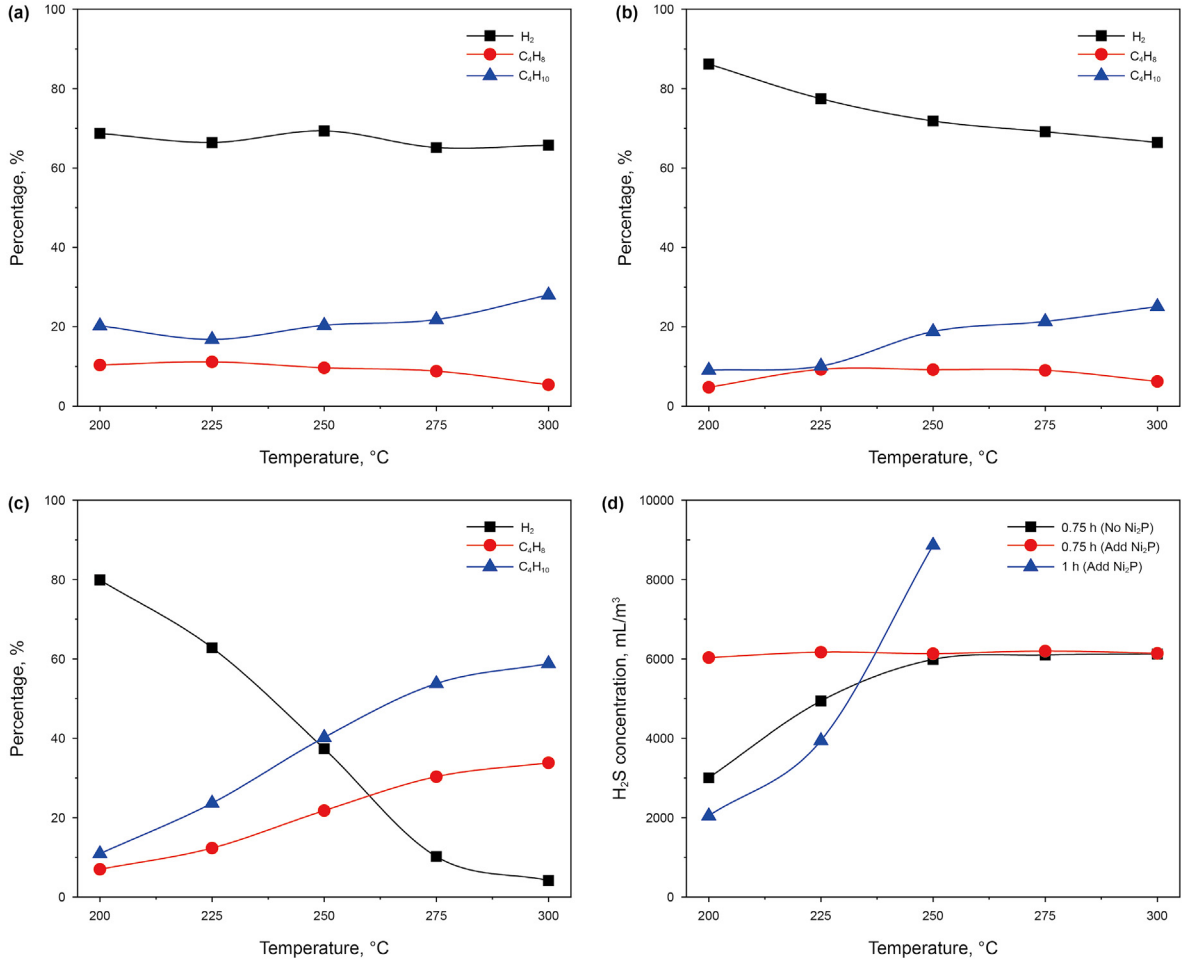

Fig.8. Percentage of gas products of THT HDS (a.0.75 h (No Ni_2P) b.0.75 h (Add Ni_2P) c.1 h (Add Ni_2P) d.H_2S concentration).

adsorption mode. The C—S bond length of tetrahydrothiophene increases, which are conducive to the breaking of the C—S bond and HDS reaction. On the contrary, the C—C bond of tetrahydrothiophene molecule is shortened after adsorption, and the C—C bond can be increased to make it more stable. It speculates that the C—S bond will break preferentially (Venezia et al., 2009).

(2) Charge population analysis

The side view and top view of the optimized adsorption configuration are shown in Fig. 11. The C2—C3 bond of tetrahydrothiophene is significantly twisted after adsorption. Mulliken population analysis is used to analyze the adsorption strength between Ni_2P and tetrahydrothiophene in order to further study the

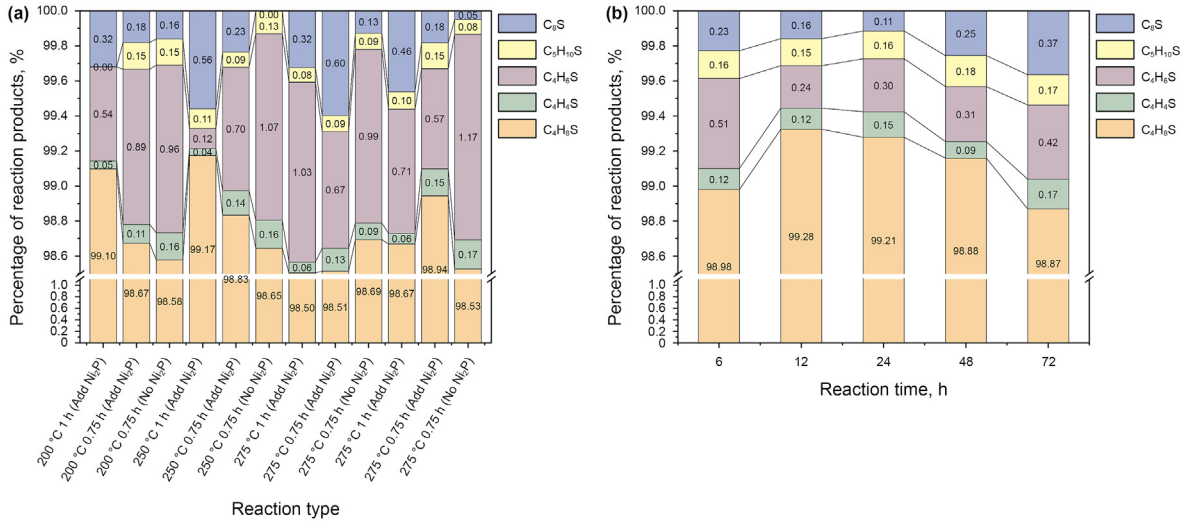

Fig.9. Analysis of tetrahydrothiophene in liquid phase (a. HDS, b. Thermal cracking (250 °C)).

adsorption behavior of Tetrahydrothiophene on Ni_2P (001) surface. The calculation result is shown in Table 1.

In the free tetrahydrothiophene molecule, the sulfur atom has a negative charge of 0.298 e, C1 and C4 have negative charge of 0.106 e, C2 and C3 have a negative charge of 0.161 e. The negative charge of Cl and C4 are less than that of C2 and C3 because of the electron-withdrawing effect of the sulfur atom. The hydrogen atoms on the ring have positive charges, and finally the charge of tetrahydrothiophene molecule in the free state is 0. When tetrahydrothiophene adsorbs on Ni_2P (001) surface, S and H loss electrons and C gets electrons. The overall charge increases to 0.256 e, showing that electrons are transferred to Ni_2P (001) surface.

Then the differential charge density was calculated. As shown in Fig. 12, Fig. 12a shows the differential charge density of tetrahydrothiophene, Fig. 12b shows the differential charge density map of corresponding section after hidden atom. The cross-section is made through S atom, C1, C2 and C4 atom. The blue area represents the loss of electrons, the red area represents the obtained electrons, and the white area represents the region where the electron density has little change. It can be seen that the C bonded with S phase has obvious electron enrichment, which is consistent with the Mulliken population analysis result.

(3) Adsorption of H_2 on Ni_2P (001)

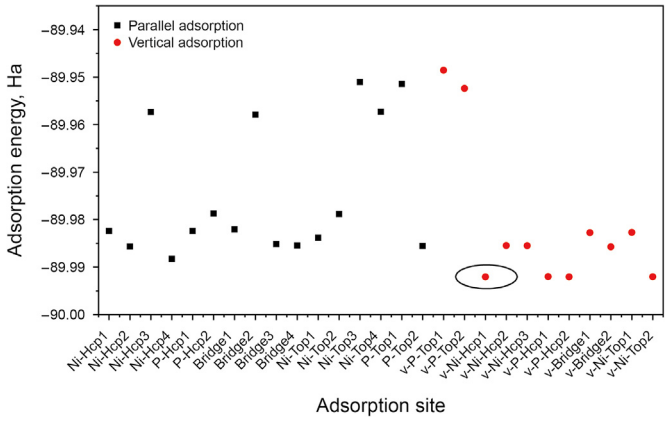

Fig.10. Adsorption energy of THT molecule Ni_2P (001) surface.

The dissociation mechanism of hydrogen on Ni_2P surface was studied. The calculated results show that the energy of a single hydrogen molecule is −1.667 Ha. H_2 dissociates at the Ni-Top position and the dissociation energy barrier is 0.073 Ha, about 2 eV. This reaction can take place at room temperature. Therefore, the reaction process of tetrahydrothiophene HDS is calculated by using H atom as reactant.

3.2.2. *Hydrogenation mechanism of tetrahydrothiophene on Ni_2P (001) surface*

The addition of H atom at different positions of tetrahydrothiophene is considered in order to determine the most reasonable reaction route (Jaf et al., 2018). The possible reaction mechanisms of seven kinds are listed in Table .2. Mechanism a is DDS and b-g are HYD. The main difference is the position of hydrogenation. Table .3 shows the activation energy *Ea* and the change of reaction energy ΔE of each step.

The Energy profiles of HDS process of THT on Ni_2P (001) surface are shown in Fig. 13, Fig. 13a shows the energy changes of the reaction a, b, c, Fig. 13b shows the energy changes of the reaction d, e, f, g. The first step of the reaction routes a, b and c are the addition of hydrogen atom to the sulfur atom. Hydrogen atom requires 5.32 eV activation energy and absorbs 1.20 eV energy. The C2—C3 bond is shortened from 1.549 Å to 1.409 Å. The second step of the route a shows that C_4H_8* is unstable and isomerize when H_2S is produced. Then the hydrogen atoms on β-C are transferred to adjacent α-C. The C2—C3 single bond becomes a double bond, and 2-butene is eventually produced. The length of C═C double bond becomes 1.387 Å, which is closer to the length of C═C double bond (1.340 Å) in common organic groups. Hydrogen atom requires 7.46 eV activation energy and absorbs 3.10 eV energy. Therefore, the potential energy of the route a is 4.30 eV, and the second step is the rate-limiting step.

The second step of the routes b and c are from RS1 to RS3. The carbon chain extends and changes from vertical adsorption to parallel adsorption after the C—S bond broke. It becomes saturated hydrocarbon after C1 obtains the hydrogen atom, and the sulfur atom is adsorbed from the Hcp site to the Top site. Due to the action of hydrogen atom in the first step, this process only requires to overcome 2.73 eV energy barrier.

The third step of the route b is from RS3 to RS4. —SH adsorbs at the Top site. The first hydrogenated C1 atom rises, and butane tends

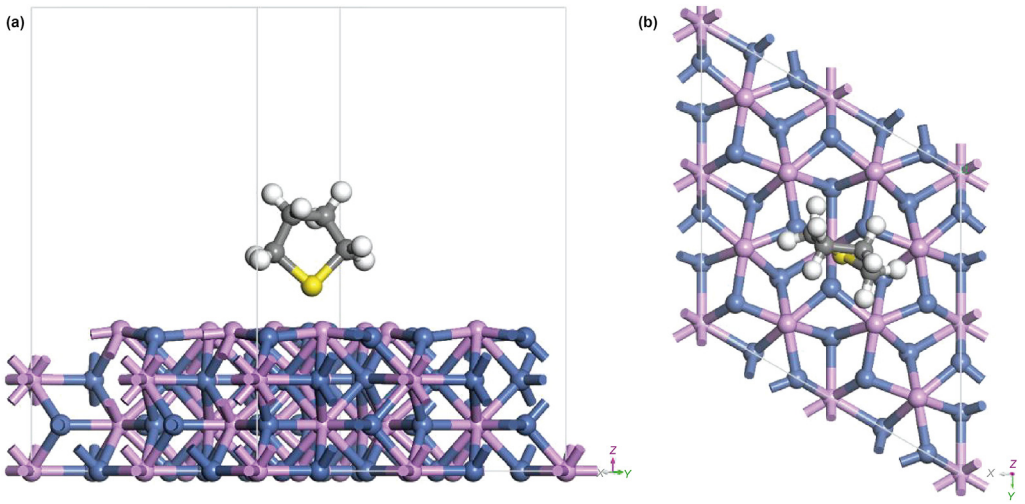

Fig.11. The side view (a) and top view (b) of THT after adsorption on Ni_2P (001).

Table 1
Mulliken charges of THT at optimal adsorption site.

Atom	*Charge, e*	
	THT	THT on Ni_2P (001)
S	−0.298	−0.162
C1	−0.106	−0.187
C2	−0.161	−0.188
C3	−0.161	−0.193
C4	−0.106	−0.180
H11	0.109	0.163
H12	0.109	0.172
H21	0.099	0.123
H22	0.099	0.133
H31	0.099	0.132
H32	0.099	0.128
H41	0.109	0.149
H42	0.109	0.166
Total	0.000	0.256

to dissociate from Ni_2P (001) surface. The process requires 4.99 eV activation energy and releases 3.10 eV energy. The third step of the route c is from RS3 to RS5. −SH hydrogenation generates H_2S, and it is far away from Ni_2P (001) surface. The bond length of Ni−S is 2.432 Å, which is larger than the bonding distance of 2.190 Å, and H_2S begins to desorb. The hydrogen atom requires 3.43 eV activation energy and absorbs 1.71 eV energy.

The first step of the reaction routes d, e, f and g are from RS1 to RS6. The hydrogen atom requires 6.17 eV activation energy and absorbs 1.59 eV energy. The second step of the route d and e is from RS6 to RS3. Unsaturated S atom begins to hydrogenate. The second step of the routes d and e are from RS6 to RS3, hydrogenation of unsaturated S atom. The hydrogen atom requires 2.34 eV activation energy and absorbs 1.21 eV energy. The second step of the route f is from RS6 to RS7. Sulfur atom is hydrogenated, and C−S bond is broken. S atom changes from the original Hcp adsorption site to −SH with the S end adsorbed at the Top site. The second step of the route g is from RS6 to RS8. Butane is produced, which is far away from Ni_2P (001) surface. S atom is adsorbed at Hcp site. This step requires 3.08 eV activation energy and absorbs 1.49 eV energy.

The activation energies of the first step of reaction routes a, b and c are 5.32 eV, which is lower than 6.17 eV of the reaction routes d, e, f and g. However, the activation energy of the second step reaction of route a is 7.46 eV, which is obviously higher than that of other reaction steps. The activation energy of the third step of the reaction routes b and c is 4.99 eV and 3.43 eV respectively, so the rate-controlling step of routes b and c are from the initial state of the first step to RS1, and the activation energy of the second step of

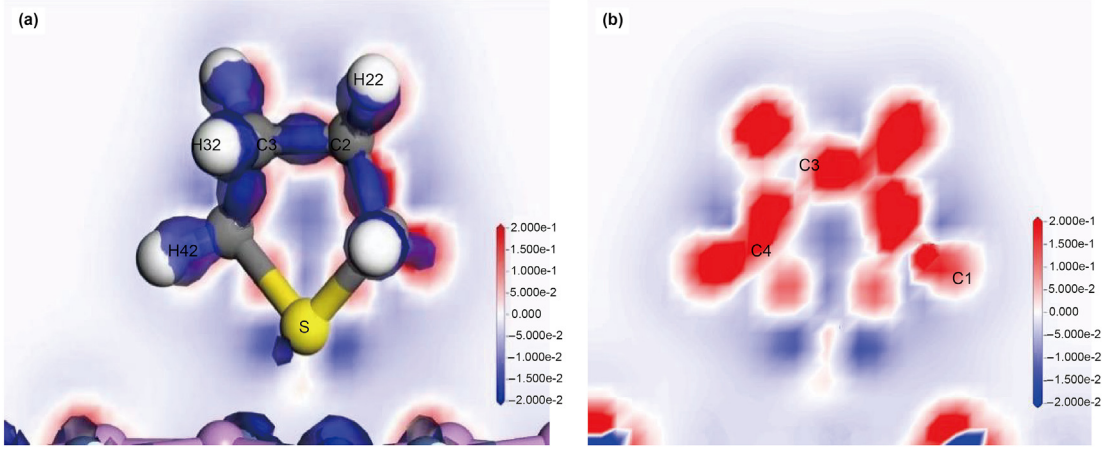

Fig.12. Differential charge density of THT adsorbed on Ni_2P (001) surface.

Table 2
Reaction mechanisms of a-g for HDS of THT on Ni_2P (001).

Step M	1	2	3
a	$C_4H_8S+H^*\rightarrow C_4H_8SH^*$	$C_4H_8SH^*+H^*\rightarrow {}^*C_4H_8{}^*+H_2S$	
b	$C_4H_8S+H^*\rightarrow C_4H_8SH^*$	$C_4H_8SH^*+H^*\rightarrow C_4H_9SH$	$C_4H_9SH+H^*\rightarrow C_4H_{10}+SH^*$
c	$C_4H_8S+H^*\rightarrow C_4H_8SH^*$	$C_4H_8SH^*+H^*\rightarrow C_4H_9SH$	$C_4H_9SH+H^*\rightarrow C_4H_9{}^*+H_2S$
d	$C_4H_8S+H^*\rightarrow C_4H_9S^*$	$C_4H_9S^*+H^*\rightarrow C_4H_9SH$	$C_4H_9SH+H^*\rightarrow C_4H_{10}+SH^*$
e	$C_4H_8S+H^*\rightarrow C_4H_9S^*$	$C_4H_9S^*+H^*\rightarrow C_4H_9SH$	$C_4H_9SH+H^*\rightarrow C_4H_9{}^*+H_2S$
f	$C_4H_8S+H^*\rightarrow C_4H_9S^*$	$C_4H_9S^*+H^*\rightarrow C_4H_9{}^*+SH^*$	
g	$C_4H_8S+H^*\rightarrow C_4H_9S^*$	$C_4H_9S^*+H^*\rightarrow C_4H_{10}+S^*$	

Table 3
Activation energy and reaction energy of each reaction on Ni_2P (001).

Route	Reaction	E_a, eV	ΔE, eV
RS1	$C_4H_8S+H^*\rightarrow C_4H_8SH^*$	5.32	1.20
RS1-RS2	$C_4H_8SH^*+H^*\rightarrow {}^*C_4H_8{}^*+H_2S$	7.46	3.10
RS1-RS3	$C_4H_8SH^*+H^*\rightarrow C_4H_9SH$	2.73	1.60
RS3-RS4	$C_4H_9SH+H^*\rightarrow C_4H_{10}+SH^*$	4.99	−1.88
RS3-RS5	$C_4H_9SH+H^*\rightarrow C_4H_9{}^*+H_2S$	3.43	1.71
RS6	$C_4H_8S+H^*\rightarrow C_4H_9S^*$	6.17	1.59
RS6-RS3	$C_4H_9S^*+H^*\rightarrow C_4H_9SH$	2.34	1.21
RS6-RS7	$C_4H_9S^*+H^*\rightarrow C_4H_9{}^*+SH^*$	1.72	0.13
RS6-RS8	$C_4H_9S^*+H^*\rightarrow C_4H_{10}+S^*$	3.08	1.49

the route b is higher than that of the route c. In comparison, the activation energy of the second step of the reaction route f is significantly lower than that of the reaction routes d, e, g and h, which is only 1.72 eV.

Therefore, the comparison of activation energy indicates that routes c and f are the most likely HDS reaction routes of Tetrahydrothiophene on Ni_2P (001) surface. The reaction mechanisms are shown in Fig. 14 and Fig. 15. The other reaction processes are shown in Appendix Fig. s2.

The reaction step of route c is the hydrogen atom combined with the broken S. Then the hydrogen atom combines with the broken α-C to make the carbon chain saturated, and eventually the hydrogen atom attacks the C—S bond to form H_2S. The reaction step of route f is the hydrogen atom first binds to the fractured α-C to make the carbon chain saturated. In the presence of hydrogen, —SH migrates to the Ni-Top site and continues to combine with the surrounding hydrogen atoms to form H_2S, while the carbon chain combines with the hydrogen atom to form butane.

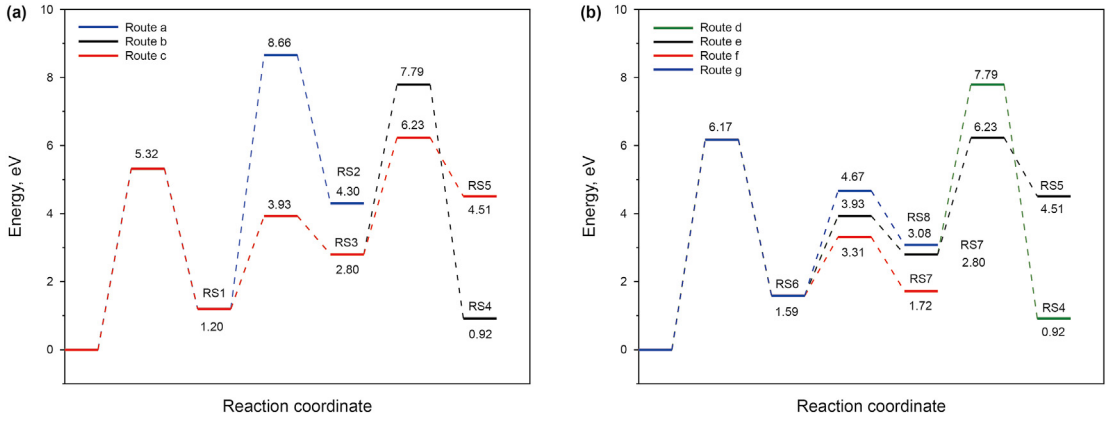

Fig.13. Energy profiles of HDS process of THT on Ni_2P (001) (a. Route a-c b. Route d-f).

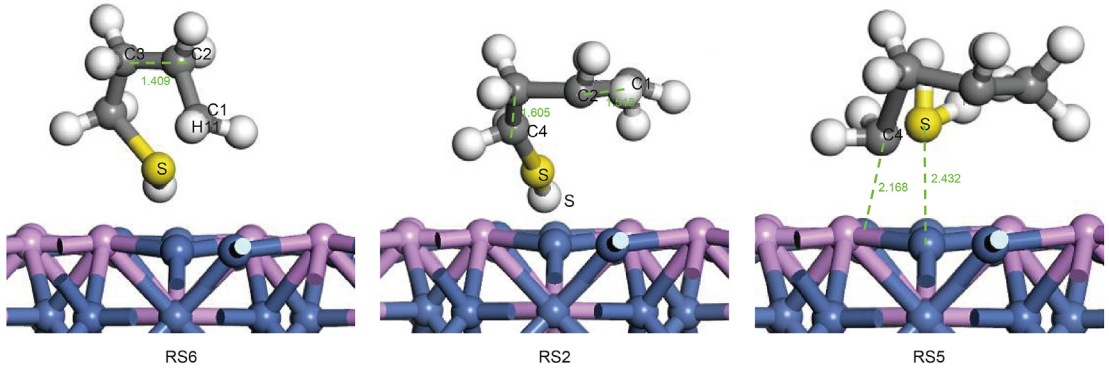

Fig.14. HDS process of THT on Ni_2P (001) (Reaction route c).

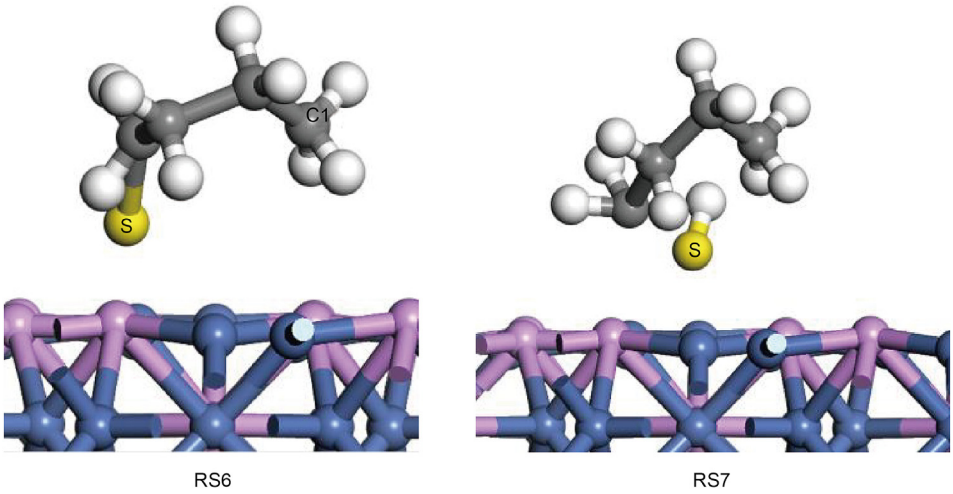

Fig.15. HDS process of THT on Ni_2P (001) (Reaction route f).

4. Conclusion

The experiment is carried out to study the thermal cracking and hydrodesulfurization of tetrahydrothiophene catalyzed by Ni_2P at 200–300 °C. The HDS reaction mechanism of tetrahydrothiophene on Ni_2P (001) surface is calculated based on Density Functional Theory. The results will provide a theoretical basis for desulfurization and viscosity reduction in the heavy oil exploitation. The main conclusions are listed below.

(1) The experiment shows that the rate of H_2S production by thermal cracking of tetrahydrothiophene is far lower than that of HDS in the range of 200–300 °C, and the HDS reaction is dominates. The major gas products are butane, butene and H_2S in HDS reaction. The liquid product in HDS reaction comes from thermal cracking of tetrahydrothiophene.

(2) The V–Ni-Hcp1 adsorption energy is larger, and the adsorption model is more stable in the vertical adsorption mode. The C–S bond is elongated, and the C–C bond is shortened after adsorption.

(3) The Mulliken charge distribution and differential charge density analysis shows that electrons are transferred to Ni_2P (001) surface through tetrahydrothiophene molecule in the adsorption process. The polarity of C–S bond is strong, and the electron shift between carbon and sulfur is obvious.

(4) HYD is the most possible route of tetrahydrothiophene on Ni_2P (001) surface, which can be divided into two reaction routes. The first reaction route is $C_4H_8 \rightarrow C_4H_8SH^* \rightarrow C_4H_9SH^* \rightarrow C_4H_{10}+H_2S$. The hydrogen atom binds to the broken S, and then binds to the broken α-C to saturate the carbon chain. Finally, the hydrogen atom attacks the C–S bond to form H_2S. The second reaction route is $C_4H_8S \rightarrow C_4H_9S^* \rightarrow C_4H_9^*+SH^* \rightarrow C_4H_{10}+H_2S$. In the presence of hydrogen, –SH migrates to the Ni-Top position and binds to the hydrogen atoms to form H_2S. The carbon chain binds to the hydrogen atom to form butane. The main products are butane and H_2S, which is consistent with the experimental results.

Acknowledgements

The authors would like to acknowledge the financial support provided by the National Science and Technology Major Project of the Ministry of Science and Technology of China (2016ZX05012-002-005), National Natural Science Foundation of China (No. 51874333) and Natural Science Foundation of Shandong Province, China (No. ZR2017MEE030).

Appendix A. Supplementary data

Supplementary data to this article can be found online at https://doi.org/10.1016/j.petsci.2021.10.023.

References

Ahmed, K.W., Ali, S.A., Ahmed, S., Al-Saleh, M.A., 2011. Simultaneous hydrodesulfurization of benzothiophene and dibenzothiophene over $CoMo/Al_2O_3$ catalysts with different [Co/(Co+Mo)] ratios. React. Kinet. Mech. Catal. 103 (1), 113–123. https://doi.org/10.1007/s11144-011-0288-1.

Bando, K.K., Wada, T., Miyamoto, T., Miyazaki, K., Takakusagi, S., Koike, Y., et al., 2012. Combined in situ QXAFS and FTIR analysis of a Ni phosphide catalyst under hydrodesulfurization conditions. none J. Catal. 286, 165–171. https://doi.org/10.1016/j.jcat.2011.10.025.

Boukoberine, Y., Hamada, B., 2016. Thiophene hydrodesulfurization over CoMo/Al_2O_3-CuY catalysts: temperature effect study. Arabian J. Chem. 9, S522–S527. https://doi.org/10.1016/j.arabjc.2011.06.018.

Clark, B.D., Hyne, J.B., 1990. Studies on the chemical reactions of heavy oils under steam stimulation condition. AOSTRA J. Res. 29 (6), 29–39.

Da Silva Neto, A.V., Leite, E.R., Da Silva, V.T., Zotin, J.L., Urquieta-Gonzalez, E.A., 2016. NiMoS HDS catalysts - the effect of the Ti and Zr incorporation into the silica support and of the catalyst preparation methodology on the orientation and activity of the formed MoS_2 slabs. Appl. Catal. A Gen.: In. J. Devoted Catal. Sci. Appl. 528, 74–85. https://doi.org/10.1016/j.apcata.2016.09.019.

Ge, Q., Jenkins, S.J., King, D.A., 2000. Localisation of adsorbate-induced demagnetisation: CO chemisorbed on Ni{110}. Chem. Phys. Lett. 327 (3–4), 125–130. https://doi.org/10.1016/S0009-2614(00)00850-2.

Gould, K.A., 1983. Influence of thermal processing on the properties of Cold Lake asphaltenes. 2. Effect of steam treatment during oil recovery. Fuel 62 (3), 370–372. https://doi.org/10.1016/0016-2361(83)90098-4.

Hyne, J.B., 1986. Aquathermolysis: a Synopsis of Work on Chemical Reaction between Water (Steam) and Heavy Oil Sands during Simulated Steam Stimulation. Canada: AOSTRA Publication Series. Alberta Oil Sands Technology and Research Authority.

Jaf, Z.N., Altarawneh, M., Miran, H.A., Jiang, Z.T., Dlugogorski, B.Z., 2018. Hydrodesulfurization of thiophene over γ-Mo_2N catalyst. Mol. Catal. 459, 21–30. https://doi.org/10.1016/j.mcat.2018.07.008.

Jin, Q., Chen, B.H., Ren, Z.B., Liang, X., Liu, N., Mei, D.H., 2018. A theoretical study on reaction mechanisms and kinetics of thiophene hydrodesulfurization over MoS_2 catalysts. Catal. Today 312, 158–167. https://doi.org/10.1016/j.cattod.2018.02.013.

Kanama, D., Oyama, S.T., Otani, S., et al., 2001. Ni_2P (0001) by XPS. Surf. Sci. Spectra 8 (3), 220. https://doi.org/10.1116/11.20020303.

Kuhn, J.N., Lakshminarayanan, N., Ozkan, U.S., 2008. Effect of hydrogen sulfide on the catalytic activity of Ni-YSZ cermets. J. Mol. Catal. Chem. 282 (1–2), 9–21. https://doi.org/10.1016/j.molcata.2007.11.032.

Lan, X.F., Hensen, E.J.M., Weber, T., 2016. Silica-supported Ni_2P: effect of preparation conditions on structure and catalytic performance in thiophene hydrodesulfurization (HDS). Catal. Today 121–132. https://doi.org/10.1016/

j.cattod.2016.12.040.
Li, G.X., Zhao, L.M., Zhu, H.Y., Liu, X.P., Ma, H.F., Yu, Y.C., et al., 2017. Insight into thiophene hydrodesulfurization on clean and S-modified MoP(010): a periodic density functional theory study. Phys. Chem. Chem. Phys. 19 (26). https://doi.org/10.1039/C7CP01859B.
Lin, R.Y., Pan, H.D., Xu, W.D., Zhang, L.Q., Wang, X.W., Zhang, J.L., et al., 2020. Hydrodesulfurization of benzothiophene on Ni_2P surface. Energy Explor. Exploit. 38 (6), 014459872094997. https://doi.org/10.1177/0144598720949976.
Liu, P., Rodriguez, J.A., 2005. Catalysts for hydrogen evolution from the [NiFe] hydrogenase to the Ni_2P (001) surface: the importance of ensemble effect. J. Am. Chem. Soc. 127 (42), 14871–14878. https://doi.org/10.1021/ja0540019.
Liu, B., Zhao, Z., Wang, D.X., Liu, J., Chen, Y., Li, T., et al., 2015. A theoretical study on the mechanism for thiophene hydrodesulfurization over zeolite L-supported sulfided CoMo catalysts: insight into the hydrodesulfurization over zeolite-based catalysts. Comput. Theor. Chem. 1052, 47–57. https://doi.org/10.1016/j.comptc.2014.12.001.
Liu, P., Rodriguez, J.A., Asakura, T., Gomes, J., Nakamura, K., 2017. Desulfurization reactions on Ni_2P(001) and alpha-Mo_2C(001) surfaces: complex role of P and C sites. J. Phys. Chem. B 109 (10), 4575–4583. https://doi.org/10.1021/jp044301x.
Ma, Q., Yang, Z.D., Zhang, L.Q., Lin, R.Y., Wang, X.W., 2019. Generation of hydrogen sulfide during the thermal enhanced oil recovery process under superheated steam conditions. RSC Adv. 9 (58), 33990–33996. https://doi.org/10.1039/C9RA07735A.
Mokheimer, E.M.A., Hamdy, M., Abubakar, Z., Shakeel, M.R., Habib, M.A., Mahmoud, M., 2019. A comprehensive review of thermal enhanced oil recovery: techniques evaluation. J. Energy Resour. Technol. 141 (3). https://doi.org/10.1115/1.4041096.
Oyama, S.T., 2003. Novel catalysts for advanced hydroprocessing: transition metal phosphides. J. Catal. 216 (1–2), 343–352. https://doi.org/10.1016/s0021-9517(02)00069-6.
Oyama, S.T., Lee, Y.-K., 2008. The active site of nickel phosphide catalysts for the hydrodesulfurization of 4,6-DMDBT. J. Catal. 258 (2), 393–400. https://doi.org/10.1016/j.jcat.2008.06.023.
Oyama, S.T., Gott, T., Zhao, H.Y., Lee, Y.-K., 2009. Transition metal phosphide hydroprocessing catalysts: a review. Catal. Today 143 (1–2), 94–107. https://doi.org/10.1016/j.cattod.2008.09.019.
Perdew, J.P., Wang, Y., 1986. Accurate and simple density functional for the electronic exchange energy: generalized gradient approximation. Phys. Rev. B 33 (12), 8800–8802. https://doi.org/10.1103/PhysRevB.33.8800.
Rundqvist, S., Yhland, M., Dahlbom, R., Sjövall, J., Theander, O., Flood, H., 1962. X-ray investigations of Mn_3P, Mn_2P, and Ni_2P. Acta Chem. Scand. 16, 992–998. https://doi.org/10.3891/acta.chem.scand.16-0992.
Sawhill, S.J., Phillips, D.C., Bussell, M.E., 2003. Thiophene hydrodesulfurization over supported nickel phosphide catalysts. J. Catal. 215 (2), 208–219. https://doi.org/10.1016/s0021-9517(03)00018-6.
Song, L.M., Zhang, S.J., Wei, Q.W., 2011. A new route for synthesizing nickel phosphide catalysts with high hydrodesulfurization activity based on sodium dihydrogenphosphite. Catal. Commun. 12 (12), 1157–1160. https://doi.org/10.1016/j.catcom.2011.03.038.
Song, H., Wang, J., Li, F., Liu, Y.X., Zhang, J.J., Song, Hl, 2013. Advance in the preparation and modification on nickel phosphide catalysts for hydrodesulfurization. Shiyou Xuebao. Acta Pet. Sin. 29 (6), 1096–1108. https://doi.org/10.3969/j.issn.1001-8719.2013.06.026 (in Chinese).
Song, H., Dai, X.Y., Zhu, T.H., Qin, H., Song, H.L., Li, F., 2019. Effect of boron promoter on structure and hydrogenation activity of Ni_2P/MCM-41 catalysts. J. China Univ. Petrol. (Edition of Natural Science) 43 (5), 170–177. https://doi.org/10.3969/j.issn.1001-8719.2015.06.004 (in Chinese).
Venezia, A.M., Murania, R., Pantaleo, G., Parola, V.L., Scirè, S., Deganello, G., 2009. Combined effect of noble metals (Pd, Au) and support properties on HDS activity of Co/SiO_2 catalysts. Appl. Catal. A Gen. 353 (2), 296–304. https://doi.org/10.1016/j.apcata.2008.11.005.
Wang, Xl, Zhao, Z., Chen, Z.T., Li, J.M., Duan, A.J., Xu, C.M., et al., 2017. Effect of synthesis temperature on structure-activity-relationship over NiMo/γ-Al_2O_3 catalysts for the hydrodesulfurization of DBT and 4,6-DMDBT. Fuel Process. Technol. 161, 52–61. https://doi.org/10.1016/j.fuproc.2017.03.003.
Wei, Q., Liu, X.D., Zhou, Y.S., Xu, Z.S., Zhang, P.F., Liu, D., 2019. A promising catalyst for hydrodesulfurization: Ni_2P – a DFT study. Catal. Today 353. https://doi.org/10.1016/j.cattod.2019.10.032.
Yi, Y.F., Li, S.Y., Ding, F.C., Yu, H., 2009. Change of asphaltene and resin properties after catalytic aquathermolysis. Petrol. Sci. 6 (2), 194–200. https://doi.org/10.1007/s12182-009-0031-y.
Zhang, F.Y., Song, H., Song, H.L., et al., 2016. Preparation of metal (Ti, Zn and Ca) modified Ni_2P catalysts and HDS performance and kinetic studies. J. Taiwan Inst. Chem. Eng. 65, 558–564. https://doi.org/10.1016/j.jtice.2016.05.048.
Zhang, J.L., Han, F., Yang, Z.D., Zhang, L.Q., Wang, X.W., Zhang, X.X., et al., 2020. Significance of aquathermolysis reaction on heavy oil recovery during steam-assisted gravity drainage (SAGD) process. Energy Fuel. https://doi.org/10.1021/acs.energyfuels.9b04004.
Zhao, P.H., Li, C.Z., Wang, C., Yang, M.L., 2016. The mechanism of H_2S generation in the recovery of heavy oil by steam drive. Liq. Fuel. Technol. 34 (16), 1452–1461. https://doi.org/10.1080/10916466.2016.1204314.
Zuriaga-Monroy, C., Martínez-Magadán, J.-M., Ramos, E., Gómez-Balderas, R., 2009. A DFT study of the electronic structure of cobalt and nickel mono-substituted MoS_2 triangular nanosized clusters. J. Mol. Catal. Chem. 313 (1/2), 49–54. https://doi.org/10.1016/j.molcata.2009.08.001.